

Abstract

A continuous-discontinuous barotropic finite element based model is developed for the simulation of synoptic scale atmospheric dynamics using the shallow

Declaration

I confirm that this work is my own and the use of all other material from other sources has been properly and fully acknowledged.

Signed

.....

Alastair J. Radcli®e

Dated

.....

Contents

Abstract	2
Declaration	3
Introduction	8
Atmospheric Model Requirements	8
Rotating Frames of Reference	9
The Material Derivative	9
The Shallow Water Equations	10
Discretization methods	11
Flow Derivative Constructions	12

.....
dehef

Test Case Seven: 500 mbar.864 Td e.5 0 Td (SGeop864 T7.0557Td (SGe5611 0 TUen502

Index of Symbols

x	Cartesian abscissa
y	Cartesian ordinate
z	Cartesian vertical coordinate
r	Spherical radial coordinate
λ	Spherical azimuth -longitude
μ	Spherical declination -latitude
i or e_x	Cartesian abscissa unit vector
j or e_y	Cartesian ordinate unit vector
k or e_z	Cartesian vertical unit vector
e_r	Spherical radial unit vector
e_λ	Spherical azimuth unit vector
e_μ	Spherical declination unit vector
r	General Position Vector
t	Time Variable
u	(Horizontal) Fluid Velocity Vector
h	Fluid (Atmospheric) Depth
ν	viscosity coefficient
ρ_0	homogeneous fluid density
h_0	Topographic Depth/Height
f	Coriolis Parameter
g	Gravitational Acceleration = 9.81 m s^{-2}
ω	Earth's Rotation Vector
a	spherical Earth radius = $6.3675 \cdot 10^6 \text{ m}$
Ω	angular rotation rate = $7.2921 \cdot 10^{-5} \text{ s}^{-1}$
H	Fluid Depth Scale Factor
H_0	Topographic Depth Scale Factor
U	Surface Fluid Velocity Scale Factor
T	Time Scale Factor
L	Surface Length Scale Factor
F	Coriolis Parameter Scale Factor
t	Dimensionless Time Coordinate
u	Dimensionless Fluid Velocity
h	Dimensionless Fluid Depth
h_0	Dimensionless Topographic Height
f	Dimensionless Coriolis Parameter
F	Dimensionless General Position Vector
R_0	Rossby Number
R_{0T}	Temporal Rossby Number

E_k	Ekman Number
-	computational domain
@-	boundary of computational domain
d_i	incremental volume element
ds	incremental surface area element
n	surface normal to @-
$\mathcal{L}^2(-)$	set of square integrable functions over -
\mathcal{H}	the set $\{h \in \mathcal{L}^2(-) : \int_{\Omega} h d_i = 0\}$
	the set $\{u \in \mathcal{L}^2(-) \cap \mathcal{L}^2(-) : u \cdot n = 0\}$
w	the set $\{u \in \mathcal{L}^2(-) \cap \mathcal{L}^2(-)\}$
»	canonical triangle abscissa
'	canonical triangle ordinate
\hat{A}_i	P_1 linear conforming shape function
\tilde{A}_i	P_1^{NC} linear non-conforming shape function
$\mathcal{L}^2(-)$	piecewise cal triangle

~
~
~

Introduction

Atmospheric Model Requirements

Given that the Earth's atmosphere is one of the most complicated dynamical systems in the universe, it is (at present) impossible to capture all its processes accurately, be they rheologic, thermodynamic and so forth, within the same computational framework. Thus it is usually necessary to consider great simplifications, whereby most of the dynamical processes of the atmosphere are ignored, and design a computational model that supports little more than the particular dynamical phenomena of interest.

Theoretically

Rotating Frames of Reference

To avoid undue complications, most atmospheric models employ a coordinate reference frame that is considered to rotate with the angular velocity representative of that of the Earth. To do otherwise would necessitate the construction of large and cumbersome expressions for quantities such as velocities, which would prove difficult to work with.

As will be indicated later, Newton's second law lies behind one of the governing equations, that relating to momentum, for the shallow water model, but is only intended to be applied in an inertial reference frame that exhibits no accelerations. The law may be applied in the non-inertial rotating reference frame, with inherent accelerations towards the centre, in the usual (inertial) manner provided two extra 'artificial' forces are included in the momentum equation derived from it.

The first of these artificial forces is usually referred to as a 'centripetal force'. It is considered to act in a direction opposite to that of gravity at every point on the Earth and is a conservative force, allowing it to be represented by a scalar gradient. Because of the centripetal forces relative weakness compared to the gravitational force, which is also conservative, it is often (and will be here to) included with it via a 'reduced' gravity potential [8].

The second artificial force is termed the 'Coriolis force' after the work of Gaspard Gustave Coriolis and is found to always act in a direction perpendicular to a given fluid element's motion [8]. As such, the force never does any work as (right hand rule) the force is always perpendicular to the direction of motion. The Coriolis force can be anticipated given its magnitude is $2\Omega \times v$ where Ω is the angular velocity of the Earth and v is the velocity of the fluid element. The Coriolis force is a vector quantity and its direction is determined by the right hand rule. The Coriolis force is a vector quantity and its direction is determined by the right hand rule. The Coriolis force is a vector quantity and its direction is determined by the right hand rule.

the position the viscous diffusion term would otherwise occupy. Ideally, and in most of what follows, the viscosity shall be considered sufficiently small for the effects of diffusion to be neglected. However, it will be seen that for some problems, a small 'artificial' diffusion is needed to stabilize the solution.

For atmospheric modelling, a 'geopotential height' is often referred to. This simply refers to the multiplication of the fluid's height (or depth), h , measured in meters, say, with the gravitational acceleration g , in meters per second squared. The units of geopotential height are thus meters squared per second squared, or $[m][m=s^2] = [m$

solution and to implement adaptive meshing techniques [17]. While such techniques have been applied recently with great success to atmospheric models [20], for the present work only linear (first-order) finite elements will be used.

Closely related to the finite element method is the 'finite volume method'. It has the same node distribution advantages of the finite element method, but works entirely in terms of the

LL

LL

17

with ~~SH~~ALLOW

For the two-dimensional case of the equations being solved here, variations in the direction given by this latter coordinate are neglected. Furthermore, in the spherical coordinate framework, the Coriolis term of the governing equations simply reads $f = 2 - \sin \mu$.

Adopting the standard right-handed spherical to cartesian coordinate transformation

$$x = r \cos \mu \cos \lambda \quad (4.1)$$

$$y = r \cos \mu \sin \lambda \quad (4.2)$$

$$z = r \sin \mu \quad (4.3)$$

the spherical unit direction vectors may be written in terms of their cartesian counterparts and a transformation matrix T as

$$\begin{pmatrix} e_r \\ e_\lambda \\ e_\mu \end{pmatrix} = \begin{pmatrix} \cos \mu \cos \lambda & \cos \mu \sin \lambda & \sin \mu \\ \sin \lambda & \cos \lambda & 0 \\ \sin \mu \cos \lambda & \sin \mu \sin \lambda & \cos \mu \end{pmatrix}^{-1} \begin{pmatrix} e_x \\ e_y \\ e_z \end{pmatrix} \quad (4.4)$$

and similarly, by inversion of the transformation matrix, the cartesian unit direction vectors may be given in terms of those for the spherical coordinate system

$$\begin{pmatrix} e_x \\ e_y \\ e_z \end{pmatrix} = \begin{pmatrix} \cos \mu \cos \lambda & \sin \lambda & \sin \mu \cos \lambda \\ \cos \mu \sin \lambda & \cos \lambda & \sin \lambda \sin \mu \\ \sin \mu & 0 & \cos \mu \end{pmatrix} \begin{pmatrix} e_r \\ e_\lambda \\ e_\mu \end{pmatrix} \quad (4.5)$$

With square braces enclosing terms that vanish for variables confined to the surface of a sphere, where all vectors are tangential to the surface, and the gradient operator in cartesian and spherical coordinates is defined as

$$\begin{aligned} &= \frac{\partial}{\partial x} e_x + \frac{\partial}{\partial y} e_y + \frac{\partial}{\partial z} e_z \\ &= \end{aligned} \quad (4.6)$$

The terms proportional to $1/r$ give rise to what are often called 'curvature terms' when these expressions are used in the governing equations because they arise due to the curvature of the earth [15]. These terms can be important where there is a combination of both high latitudes and strong atmospheric flows.

It will be useful to consider those derivatives of the normalised spherical basis vectors with non-trivial results. With respect to λ ,

$$\begin{aligned} \frac{\partial}{\partial \lambda} \begin{pmatrix} e_r \\ e_\lambda \\ e_\mu \end{pmatrix} &= \begin{pmatrix} \cos \mu \sin \lambda & \cos \mu \cos \lambda & 0 \\ -\sin \mu \sin \lambda & -\sin \mu \cos \lambda & 0 \\ 0 & \cos \mu & -\sin \mu \end{pmatrix} \begin{pmatrix} e_r \\ e_\lambda \\ e_\mu \end{pmatrix} \\ &= \begin{pmatrix} 0 & \cos \mu & 0 \\ \cos \mu & 0 & \sin \mu \\ 0 & \sin \mu & 0 \end{pmatrix} \begin{pmatrix} e_r \\ e_\lambda \\ e_\mu \end{pmatrix} \end{aligned} \quad (4.12)$$

and then μ

$$\begin{aligned} \frac{\partial}{\partial \mu} \begin{pmatrix} e_r \\ e_\lambda \\ e_\mu \end{pmatrix} &= \begin{pmatrix} \sin \mu \cos \lambda & \sin \mu \sin \lambda & \cos \mu \\ 0 & 0 & -\sin \mu \\ \cos \mu \cos \lambda & \cos \mu \sin \lambda & \sin \mu \end{pmatrix} \begin{pmatrix} e_r \\ e_\lambda \\ e_\mu \end{pmatrix} \\ &= \begin{pmatrix} 0 & 0 & 1 \\ 0 & 0 & 0 \\ 1 & 0 & 0 \end{pmatrix} \begin{pmatrix} e_r \\ e_\lambda \\ e_\mu \end{pmatrix} \end{aligned} \quad (4.13)$$

Finally, we will need to consider the forcing term

$$\begin{aligned} \int_a^b \mathbf{a} \cdot d\mathbf{s} &= \int_a^b \frac{1}{r \cos \mu} \frac{\partial \mathbf{a}}{\partial \lambda} + \frac{1}{r \sin \mu} \frac{\partial \mathbf{a}}{\partial \mu} \cdot r^2 \cos \mu \, d\lambda \, d\mu \\ &= R \int_a^b \left(\frac{\partial \mathbf{a}}{\partial \lambda} + \cos \mu \frac{\partial \mathbf{a}}{\partial \mu} \right) \cdot d\mathbf{s} \end{aligned} \quad (4.14)$$

and the non-linear term of the momentum equation

$$\int_a^b \mathbf{a} \cdot d\mathbf{s} = \int_a^b \frac{1}{r \cos \mu} \frac{\partial \mathbf{a}}{\partial \lambda} + \frac{1}{r \sin \mu} \frac{\partial \mathbf{a}}{\partial \mu} \cdot d\mathbf{s}$$



Weak Formulations

For the mixed formulations of the shallow water equations, where both a velocity and an elevation field need to be discretized, there are two alternative weak formulations that may be found by integrating by parts different terms within either the governing mass (2.4) or momentum (2.3) equation after an appropriate arbitrary testing function has been integrated in [12].

For the momentum equation we would have

$$\int_{\Omega} \frac{Du}{Dt} \hat{u} \, d\zeta + f \int_{\Omega} k \, u \hat{u} \, d\zeta = g \int_{\Omega} (h + h_0) \hat{u} \, d\zeta \quad (5.1)$$

while for the mass equation there is

$$\int_{\Omega} \frac{\partial h}{\partial t} \hat{h} \, d\zeta + \int_{\Omega} (hu) \hat{h} \, d\zeta = 0 \quad (5.2)$$

The choice of which weak formulation to use usually depends on the continuity requirements they place on the pre-defined basis functions associated with the velocity and elevation variables.

Continuous Elevation Form

Now, the only term in these equations requiring continuity of the velocity field is the divergence term of the mass conservation equation. Integrating this term by parts will allow the continuity requirement to be shifted onto the elevation with the

One of the key features of weak formulations is the imposition of boundary conditions in an average, or weak sense, which has been shown to be preferable to a strong enforcement [13], [28]. For present purposes, that means removing the integrals of u_n and u_n on the domain boundary -the latter will be seen to arise in considerations of the viscous term.

Th

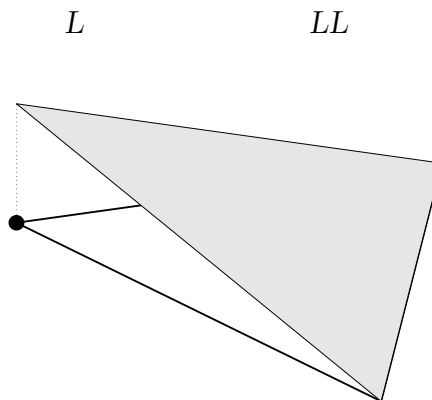


Figure 2: Linear Conforming Basis Function over Triangular Finite Element

allows the non-linear contribution to be formed

$$\int_{\Omega} \frac{1}{2} \frac{\partial \mathbf{u}}{\partial t} \cdot \mathbf{u} + \mathbf{f} \cdot \mathbf{k} \cdot \mathbf{u} \, d\zeta + \int_{\partial\Omega} (\mathbf{u} \cdot \mathbf{n}) \mathbf{u} \, d\zeta = \int_{\Omega} \mathbf{g} \cdot (\mathbf{h} + \mathbf{h}_0) \cdot \mathbf{u} \, d\zeta \quad (5.9)$$

Finite Element Spatial Discretization

To derive the finite element discretization of the governing equations, we first introduce a discretization of the domain Ω into triangles T_e ($1 \leq e \leq N_E$). This triangulation is composed of N_{Γ} interelement segments Γ_{ef} with $e > f$. Each Γ_{ef} is associated with a unique normal vector \mathbf{n} which points from T_e to T_f . The total number of segments and vertices in the triangulation are respectively denoted N_S and N_V .

Discrete finite element equations are then found by approximating the elevation and velocity fields by summations of linear conforming, P_1 , and linear non-conforming, P_1^{NC} , basis functions respectively.

Linear Conforming Basis Functions

The three linear conforming basis functions for the canonical triangular element are given by

$$\hat{A}_1(\boldsymbol{\eta}; \boldsymbol{\zeta}) = 1 - \eta_1 \quad (6.1)$$

$$\hat{A}_2(\boldsymbol{\eta}; \boldsymbol{\zeta}) = \eta_2 \quad (6.2)$$

$$\hat{A}_3(\boldsymbol{\eta}; \boldsymbol{\zeta}) = \eta_3 \quad (6.3)$$

where it should be noted

$$\hat{A}_1 + \hat{A}_2 + \hat{A}_3 = 1 \quad (6.4)$$

One such basis function may be seen for the general triangular finite element in Figure 2.

for the zonal component, and

$$\begin{aligned} \frac{dv_j}{dt} &= a^2 \int_{\Omega} \tilde{A}_i \tilde{A}_j \cos \mu \, d_s \, d\mu + \int_{\Omega} \frac{\partial \tilde{A}_k}{\partial \mu} \tilde{A}_i \tilde{A}_j \cos \mu \, d_s \, d\mu + \int_{\Omega} v_j v_k a \frac{\partial \tilde{A}_k}{\partial \mu} \tilde{A}_i \tilde{A}_j \cos \mu \, d_s \, d\mu \\ &+ u_j a^2 \int_{\Omega} f \tilde{A}_i \tilde{A}_j \cos \mu \, d_s \, d\mu = g (h_j + h_{0j}) a \int_{\Omega} \tilde{A}_i \frac{\partial \tilde{A}_j}{\partial \mu} \end{aligned}$$

where a comparable notation of n_{ij} has been used for the coefficient of the time derivative for the mass equation.

Again, accumulating all such integrals over elements of the computational domain allows us to introduce the right hand side term b_h

$$n_{ii} \frac{\partial h_i}{\partial t} = b_h \quad (7.11)$$

where to achieve the same simple structure for the elevation mass equation (7.10), given that the conforming basis functions used for the elevation field are not orthogonal, the equiv

in equations (7.5) and (7.6). Without loss of generality, we shall consider the normal derivative term, similar arguments may be made for the other upwinded terms.

Consider the sum of two such boundary integrals appearing in the full discretized zonal momentum equation for the whole computational domain, and arising from the integrations over two neighbouring elements labelled i and j with boundaries $\partial\Omega_i$ and $\partial\Omega_j$ respectively.

$$\int_{\partial\Omega_i} \frac{\partial \mathbf{u}^h}{\partial \mathbf{n}_i} [:::] ds + \int_{\partial\Omega_j} \frac{\partial \mathbf{u}^h}{\partial \mathbf{n}_j} [:::] ds \quad (7.13)$$

Let the shared side between such elements be denoted by Γ_{ij} with the subscript order indicating the direction in which the segment is to be traversed and with a normal \mathbf{n}_i pointing away from element i into element j and a normal \mathbf{n}_j pointing away from element j into element i . Then the contributions to the last sum from this edge will be

$$\int_{\Gamma_{ij}} \frac{\partial \mathbf{u}^h}{\partial \mathbf{n}_i} [:::] ds + \int_{\Gamma_{ji}} \frac{\partial \mathbf{u}^h}{\partial \mathbf{n}_j} [:::] ds \quad (7.14)$$

To avoid a spurious build up of mass along the interface between the two elements, we would expect

$$\frac{\partial \mathbf{u}^h}{\partial \mathbf{n}_i} = \frac{\partial \mathbf{u}^h}{\partial \mathbf{n}_j} \quad (7.15)$$

considering that the normals are in opposite directions.

To enforce this continuity restraint it is necessary to decide how the different values of $\frac{\partial \mathbf{u}^h}{\partial \mathbf{n}}$ inside each of the two elements are to contribute to this shared value. This bias may be summarised with a parameter α such that the flux over the interface is given by

$$\frac{\partial \mathbf{u}^h}{\partial \mathbf{n}} = (1 - \alpha) \frac{\partial \mathbf{u}^h}{\partial \mathbf{n}_i} + \alpha \frac{\partial \mathbf{u}^h}{\partial \mathbf{n}_j} \quad (7.16)$$

where the 'downwind' and 'upwind' subscripts indicate the elements into which there is a net flow in and out of the element respectively.

There has been much work on the exact choice that

wavelengths smaller than the typical grid element dimensions, such upwinding can be seen as a sub-grid scale model [14].

Artificial Diffusion

Although the use of non-conforming basis functions for velocity fields is known to dissipate high order oscillations within a solution [14], and even with fully upwinded equations, numerical instabilities in the solution can still set in.

In common

Numerical Experiments

Introduction

For the validation of the code as adapted to a spherical geometry, a number of test cases suggested by Williamson et al. [29], appropriate to the use of the shallow water equations on a sphere, was considered. These tests started from relatively simple experiments to validate the purely advective properties of the code, by resetting the winds to the initial values every timestep and observing the propagation of a Cosine Bell disturbance (test case 1), to the much more sophisticated replication of gravity waves excited by an isolated mountain (test case 5) and approximations to the Rossby-Haurwitz waves. The latter are actually analytic solutions to the non-linear barotropic vorticity equation (derived from the shallow water equations) on the sphere, but which may be approximated in the shallow water model (test case 6).

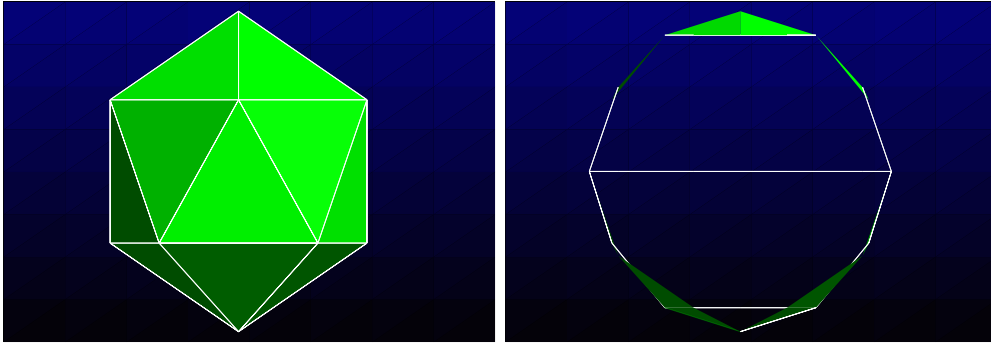
In the following, solutions for test cases 1,5,6 and 7 of [29] were generated, the last test being liberally interpreted as simply running the numerical model on a realistic data set (taken for current purposes from the ECMWF archives). The test cases 2,3 and 4 would appear to be less popular in the literature, are thus harder to find comparisons for, and are not reported here. A structured mesh generator was developed to create meshes of various different sizes (in terms of the number of elements they consisted of), with a very uniform element size distribution as can be seen in the sequence shown in Figure 4.

The largest of these structured meshes, with 20480 elements, was used to capture the dissipative processes and steep velocity gradients of test cases 1 and 5. The initial conditions of test case 1 may be seen on this mesh in Figure 5. However, a much smaller structured mesh of 8192 elements, derived from recursion of the icosahedron, was tried for the simpler test case 6 anticipating the solution's smoother behaviour.

The last test case, employing actual data, was initially

LL

33



where the parameter θ corresponds to the angle between the axis of solid body rotation and the polar axis of the spherical coordinate system and allows for the direction of advection to be varied to test the isotropy of the method and/or mesh considered [29]. For the solution presented here this is kept at zero, giving rise to an advection around the equator.

The initial cosine bell test pattern that is to be advected is given by

$$h(\lambda; \mu) = \frac{h_0}{2} \left[1 + \cos\left(\frac{\pi r}{R}\right) \right] \quad (8.2)$$

for $r < R$, and $h(\lambda; \mu) = 0$ otherwise, where $h_0 = 1000\text{m}$ and r is the great circle distance between $(\lambda; \mu)$ and the center of the mountain, initially taken as $(\lambda_c; \mu_c) = (3\frac{1}{4}\pi; 0)$, and is given by

$$r = a \cos^{-1} [\sin \mu_c \sin \mu + \cos \mu_c \cos \mu \cos(\lambda - \lambda_c)] \quad (8.3)$$

The radius $R = a=4$ and the advecting wind velocity is given by

$$u_0 = \frac{2\frac{1}{4} a}{12 \text{ days}} \quad (8.4)$$

which corresponds to about 40 m/s. No artificial viscosity was introduced for this test case.

As can be seen in Figure 6, there appears to be a slight loss in height of the initial disturbance, and a large associated 'dip' behind, as it propagates around the Earth. This can be attributed to the limitations the conforming basis functions have when advecting the elevation field. Because these continuous functions take information from neighbouring elements isotropically, their performance may be described as centered.

Ideally such advection of the elevation field would be dealt with purely 320940-0-0-0 (b)1

Test Case Five: Zonal Flow over an Isolated Mountain

This test case again consists of a solid body rotation or zonal flow

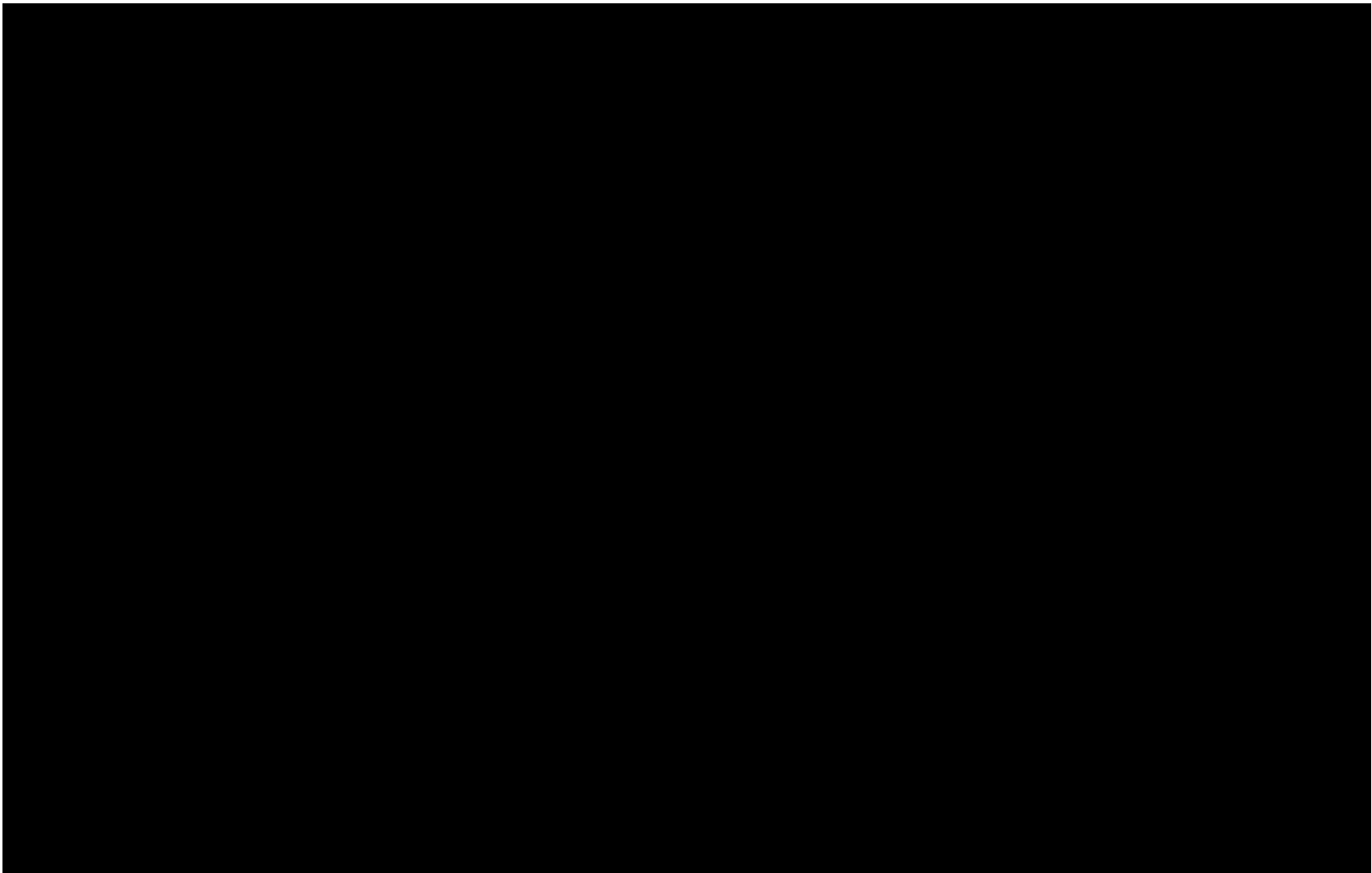
$$\mathbf{u} = u_0 (\cos \mu \cos \theta + \sin \mu \cos \lambda \sin \theta) \mathbf{W} \mathbf{F} \mathbf{l} \mathbf{o}$$

indicates the exact time for which the 500 mbar initial data used correspond, namely midnight before the first day of November 2001.

Figures 11 and 12 show contour plots of the geopotential height evolved from the 500mbar initial data at roughly daily intervals for the following 5 days, with a diffusion of $2 \times 10^6 \text{ m}^2\text{s}^{-1}$ used to stabilize the results.

Owing to the relative coarseness of the mesh used it is difficult to pick out anything but the most large-scale trends in the synoptic behaviour, though a developing wave may be seen to start propagating westwards in the elevation data around the south pole.

It should be noted that data could only be extracted from the encoded ECMWF files in the form of values on a 'lat-long' (latitude-longitude) grid. Thus it wa





LT



LT

42

L

LL





44

L

LL

1.57

0.785

0

-0.785

-1.57

-3.14

-1.57

4.63e+003

0

5.21e+003

1.57

5.79e+003

3.14



LL

45

1.57

0.785

0

-0.785

-1.57

-3.14

-1.57

4.61e+003

0

5.22e+003

1.57

5.83e+003

3.14



formula, with no need to simply 'hope' that things won't blow up.

Of course, with respect to the results of test case 7, improved results could more immediately be obtained if the problems simply with the interpolations to get the initial data could be overcome, or circumvented. It would also be interesting if a whole sequence of, perhaps daily, real weather data could be extracted from archives with which to compute the L_2 errors of the global elevation and velocity fields as the solution time progresses from that corresponding to the initial data.

Finally, although the use of non-conforming basis functions for velocity fields and full upwinding of the momentum equation is known to dissipate high order oscillations within a solution, it was still found necessary to introduce a general diffusion term to smooth some of the solutions and act against the creation of local velocity extrema. The use and application of this artificial diffusion, however, could also be improved.

The principal attraction of introducing viscosity to an otherwise inviscid problem is to 'smear' out steep velocity (or elevation) gradients which could otherwise give rise to short wavelength instabilities that can initiate the destruction of the solution. However, at present, the code associated with this work applies diffusion in a uniform manner, so smearing is performed globally on the whole solution regardless of whether or not there happens to be a steep solution gradient at a particular location.

Given that the presence of diffusion tends to decrease the overall energy contained within a solution, violating any energy conservation principle, it has been suggested [24], that a more sophisticated application of diffusion, only increasing the viscosity in regions of high shear, could achieve the same results in terms of increased stability through the diffusion of high-order modes, but with a lot less energy loss.

Implementing such a scheme could be relatively easy, with simply the need to establish some form of linear, or otherwise, dependence of the viscosity to be applied at a given location to the elevation or velocity gradients (or a combination of both) there.

References

- [1] A. Arakawa. Computational design for long-term numerical integration of the equations of fluid motion: Two-dimensional incompressible flow. Part I. *Journal of Computational Physics*, 1:119{143, 1966.
- [2] M. Baines. *Moving Finite Elements*. Oxford Uni. Press, 1994.
- [3] L. Bonaventura, L. Kornbluh, T. Heinze, and P. Ripodas. A semi-implicit method conserving mass and potential vorticity for the shallow water equations on the sphere. *Int. J. Numer. Meth. Fluids*, 47:863{869, 2005.
- [4] J. Cote, M. Roch, A. Staniforth, and L. Fillion. A variable-resolution semi-lagrangian finite-element global model of the shallow-water equations. *Mon. Weath. Rev.*, 121:231{243, 1993.
- [5] M.J.P. Cullen. Integrations of the primitive equations on a sphere using the finite element method. *Quart. J. Roy. Meteorol. Soc.*, 100:555{562, 1974.
- [6] M.J.P. Cullen. On the use of artificial smoothing in galerkin and finite difference solutions of the primitive equations. *Quart. J. Roy. Meteorol. Soc.*, 102:77{93, 1976.
- [7] M.J.P. Cullen. Forecasting and general circulation results from finite element models. *Quart. J. Roy. Meteorol. Soc.*, 105:571{592, 1979.
- [8] B. Cushman-Roisin. *Introduction to geophysical fluid dynamics*. -. Prentice-Hall, 1994.
- [9] D.R. Durran. The third-order adams-bashforth method: An attractive alternative to leapfrog time differencing. *Mon. Weath. Rev.*, 119:702{720, 1991.
- [10] D.R. Durran. *Numerical methods for wave equations in geophysical fluid dynamics*. Springer Press, 1999.
- [11] A. Fournier, M.A. Taylor, and J.A. Tribbia. The spectral element atmosphere model (seam): High-resolution parallel computation and localized resolution of regional dynamics. *Mon. Weath. Rev.*, 132:726{748, 2004.
- [12] E. Hanert. *Towards a Finite Element Ocean Circulation Model*. PhD thesis, Universit  catholique de Louvain, Belgium, 2004.
- [13] E. Hanert and V. Legat. How to save a bad element with weak boundary conditions. *Computers and Fluids*, 35:477{484, 2006.
- [14] E. Hanert, D.Y. LeRoux, V. Legat, and E. Deleersnijder. Advection schemes for unstructured grid ocean modelling. *Ocean Modelling*, 7:39{58, 2004.

- [15] J.R. Holton. *An introduction to dynamic meteorology*. -. Academic Press, 1979.
- [16] Y. Kurihara. Numerical integration of the primitive equations on a spherical grid. *Mon. Weath. Rev.*, 93:399{415, 1965.
- [17] M. Lauter and D. Handorf. A parallel adaptive barotropic model of the atmosphere. *J. Comp. Phys.*, 223:609{628, 2007.
- [18] M. Lauter and D. Handorf. A parallel adaptive barotropic model of the atmosphere. *J. Comp. Phys.*, 223:609{628, 2007.
- [19] D. LeRoux, E. Hanert, V. Rostand, and B. Pouliot. Impact of mass lumping on gravity and rossby waves in 2d τ -nite-element shallow-water models. *International Journal for Numerical Methods in Fluids*, Submitted:{, 2008.
- [20] M.N. Levy, D.N. Ramachandran, and H.M. Tufu. High-order galerkin methods for scalable global atmospheric models. *Computers and Geosciences*, 33:1022{1035, 2007.
- [21] S.J. Lin and R.B. Rood. An explicit σ -flux-form semi-lagrangian shallow-water model on the sphere. *Quart. J. Roy. Meteorol. Soc.*, 123:2477{2498, 1997.
- [22] F. Mesinger and A. Arakawa. *Numerical Methods used in Atmospheric Models*. GARP Publications Series No. 17. WMO - ICSU, 1976.
- [23] J. Pedlosky. *Geophysical Fluid Dynamics*. Springer Press, 1987.
- [24] J. Smagorinsky. General circulation experiments with the primitive equations. *Mon. Weath. Rev.*, 91:99{164, 1963.
- [25] A.N. Staniforth and H.L. Mitchell. A semi-implicit τ -nite-element barotropic model. *Mon. Weath. Rev.*, 105:154{168, 1977.
- [26] M. Taylor, J. Tribbia, and M. Iskandarani. The spectral element method for the shallow water equations on a sphere. *J. Comp. Phys.*, 130:92{108, 1997.
- [27] J. Thuburn. A pv-based shallow-water model on a hexagonal-icosahedral grid. *Mon. Weath. rev.*, 125:2328{2347, 1997.
- [28] J.J. Westerink, R.A. Luetich, J.K. Wu, and R.L. Kolar. The influence of normal σ ow boundary conditions on spurious modes in τ -nite element solutions to the shallow water equations. *Int. J. Numer. Meth. Fluids*, 18:1021{1060, 1994.
- [29] D.L. Williamson, J.B. Drake, J.J. Hack, R. Jakob, and P.N. Swarztrauber. A standard test set for numerical approximations to the shallow water equations in spherical geometry. *Journal of Computational Physics*, 102:211{224, 1992.